Materials Science and Engineering B 270 (2021) 115175

Contents lists available at ScienceDirect

Materials Science & Engineering B

journal homepage: www.elsevier.com/locate/mseb

Application of i-a-$Si_{1-x}O_x$:H as i/n interface layer of a-$Si_{1-x}Ge_x$:H single-junction flexible solar cell

Sorapong Inthisang [a,*], Chanarong Piromjit [b], Taweewat Krajangsang [b], Aswin Hongsingthong [b], Kobsak Sriprapha [b]

[a] Division of Physics, Faculty of Science, Nakhon Phanom University, Nakhon Phanom 48000, Thailand
[b] Solar Energy Technology Laboratory (STL), National Electronics and Computer Technology Center (NECTEC) National Science and Technology Development Agency (NSTDA), 111 Phahon Yothin Rd., Klong 1, Klong Luang, Pathumthani 12120 Thailand

ARTICLE INFO

Keywords:
Hydrogenated amorphous silicon oxide layer
Single-junction amorphous silicon germanium solar cell
Flexible solar cell
p/i interface layer
i/n interface layer

ABSTRACT

We investigated the effect of the flow rate of CO_2 on the optical and structural properties of i-a-$Si_{1-x}O_x$:H films deposited using 27-MHz very-high-frequency plasma-enhanced chemical vapor deposition. Experimental results show that with an increasing CO_2 flow rate, the optical bandgap of the film was increased due to the increase of the oxygen concentration, while the transparent result showed a higher value than the conventional a-Si:H material at long wavelength. This result indicated that the i-a-$Si_{1-x}O_x$:H is suitable for an application to the i/n interface layer of an a-$Si_{1-x}Ge_x$:H solar cell. The deposition conditions of the films were applied to the i/n interface layer of a-$Si_{1-x}Ge_x$:H single-junction flexible solar cells. It was found that the conversion efficiency of a solar cell with an i-a-$Si_{1-x}O_x$:H i/n interface layer showed a higher value due to the higher short circuit current density compared to a conventional a-Si:H i/n interface layer. In addition, with the optimum conditions of the i-a-$Si_{1-x}O_x$:H i/n interface layer, a conversion efficiency of 6.6% (V_{oc} = 0.81 V, J_{sc} = 14.6 mA/cm^2, and FF = 0.57) was achieved with a solar cell area of 1 × 1 cm^2.

1. Introduction

Hydrogenated amorphous silicon (a-Si:H) thin-film solar cells fabricated on flexible substrates are an interesting technology for solar cell manufacturing and laboratory research [1–4]. To achieve high efficiency for this type of solar cell, a stacked structure with double and triple junctions is required [5–7]. For stacked solar cells, hydrogenated amorphous silicon germanium (a-$Si_{1-x}Ge_x$:H) is a candidate material for the middle and bottom cells of triple and tandem structures, respectively. This is possible because the bandgap of this material can be tuned in the range of 1.5 to 1.8 eV by variation of the germanium (Ge) concentration [8–12]. However, for the fabrication of a high-efficiency a-$Si_{1-x}Ge_x$:H solar cell, it is widely accepted that the bandgap of the intrinsic a-$Si_{1-x}Ge_x$:H should be graded with several bandgap profiling shapes [13–18].

A thin-film silicon solar cell was fabricated on the flexible substrate is an interesting technology that still has the room for efficiency improvement in different ways. Several research groups reported a technique for efficiency improvement of this solar cell by bandgap profiling for the absorbing layer [13–18], a light trapping technique for improvement of the short-circuit current density (J_{sc}) [19,20], and modification of the p/i interface for improvement of the open-circuit voltage (V_{oc}) and the fill factor (FF) [8,21]. In the fabrication of a-$Si_{1-x}Ge_x$:H solar cells, bandgap discontinuities cause lattice mismatch between the n/i and p/i interfaces and a high defect density at these interface layers. As a result, V_{oc} and FF of the solar cell are decreased due to the reduced internal electric field and the carrier collection [8,13,21]. The optimization of the p/i interface plays a crucial role in the improvement of the a-$Si_{1-x}Ge_x$:H thin film solar cell efficiency due to the better V_{oc} and FF compared to a solar cell fabricated without the p/i interface layer [8,21].

However, it was also reported that an application of intrinsic hydrogenated amorphous silicon (i-a-Si:H) for the i/n interface layer could improve the V_{oc} and FF [13,22]. In these reports, it was concluded that the bandgap discontinuities and the lattice mismatch were improved by using a wider-bandgap material for the i/n interface layer of the a-$Si_{1-x}Ge_x$:H solar cell. A numerical simulation also supported the benefit of using a wide-bandgap i-a-$Si_{1-x}O_x$:H layer for the i/n interface layer of

* Corresponding author.
E-mail address: sorapong.inthisang@npu.ac.th (S. Inthisang).

https://doi.org/10.1016/j.mseb.2021.115175
Received 5 June 2018; Received in revised form 30 April 2020; Accepted 3 April 2021
Available online 24 April 2021

an a-Si:H solar cell due to the better V_{oc} and *FF* compared to a conventional structure [23]. In our research group, intrinsic amorphous silicon oxide (i-a-$Si_{1-x}O_x$:H) has been used for the p/i interface layer and intrinsic absorber-layer of a-Si:H-based thin-film solar cells [24,25]. Therefore, we are also interested in the role of the i/n interface when using this material with an a-$Si_{1-x}Ge_x$:H thin-film solar cell.

In this study, we investigated the optical and structural properties of i-a-$Si_{1-x}O_x$:H deposited in the same deposition chamber of n-layer by 27-MHz very-high-frequency plasma-enhanced chemical vapor deposition (VHF-PECVD). Then, the deposition conditions of the films were applied to the i/n interface of n-i-p a-$Si_{1-x}Ge_x$:H single-junction flexible solar cells. Finally, the effect of the i/n interface's layer thickness on the solar cells' performance was also investigated.

2. Experimental details

2.1. Preparation of i-a-$Si_{1-x}O_x$:H films

The i-a-$Si_{1-x}O_x$:H films were deposited on Corning 7059 glass substrates by 27-MHZ VHF-PECVD in the same deposition chamber of the n-layer. The pressure applied in the deposition chamber was on the order of 10^{-6} Torr using a turbo molecular pump backed by rotary pumps. The gas sources were silane (SiH_4), hydrogen (H_2), and carbon dioxide (CO_2). The deposition conditions for the i-a-$Si_{1-x}O_x$:H films are summarized in Table 1. Fourier-transform infrared spectroscopy (FTIR) were carried out to analyze the structural properties of the films (Perkin Elmer, Lambda 35). The refractive index (n), transmittance, and film thickness were measured by spectroscopic ellipsometry (J.A. Woollam, V-VASE series). The measurement data for E_{opt} was analyzed using the Tauc-Lorentz model [26,27].

2.2. Fabrication of n-i-p a-$Si_{1-x}Ge_x$:H single-junction flexible solar cells

The n-i-p a-$Si_{1-x}Ge_x$:H single-junction flexible solar cells were fabricated on polyimide with a size of 5 × 10 cm^2 [20]. A schematic of the solar cell structure for the flexible solar cell is shown in Fig. 5. Aluminum (Al) and silver (Ag) were deposited on the full area of the substrate by a thermal evaporator. These layers were designed for light reflection from the backside of the solar cell in order to increase the current density.

Then, the substrate was transferred to a multi-chamber PECVD system. It was preheated at 150 °C in a load lock chamber, and then zinc-oxide-doped aluminum (ZnO:Al) was deposited by magnetron sputtering in the ZnO:Al chamber. The ZnO:Al layer plays a role in light scattering and reflecting due to the roughness and the difference in the optical refractive index. As a result, with the cooperation of the Al/Ag back reflective layer and ZnO:Al layer, J_{sc} of the solar cell will be increased [28,29]. This cooperation layer is well known for light-trapping techniques for silicon-based thin-film solar cell fabrication.

Next, the n-layer, i/n interface-layer, i-layer, p/i interface-layer, and p-layer were deposited in different chambers. In this experiment, the main n-i-p structure of the solar cell consisted of n-type microcrystalline silicon oxide (n-μc-$Si_{1-x}O_x$:H)/i-$Si_{1-x}O_x$:H i/n interface-layer/VU-shape i-a-$Si_{1-x}Ge_x$:H bandgap profiling absorber-layer/ i-$Si_{1-x}O_x$:H p/i interface-layer/p-type microcrystalline silicon oxide (p-μc-$Si_{1-x}O_x$:H) were deposited by the PECVD technique. After finishing the deposition of the p-layer, the substrate was retrieved from the deposition system for the installation of the metal mask to make 5 small solar cells with an active area of 1.0 × 1.0 cm^2.

Next, the substrate was put in the load lock chamber for preheating and then moved to the ZnO:Al deposition chamber to deposit the front transparent conductive oxide (TCO) layer. After finishing the ZnO:Al front layer, the sample was moved out from the PECVD system for changing the metal mask to a grid shape. Finally, the substrate was moved to the evaporation system to make the Ag/Al front grid. The photovoltaic (PV) performance of n-i-p a-$Si_{1-x}Ge_x$:H single-junction flexible solar cells was measured under standard test conditions of AM 1.5 and 100 mW/cm^2 at 25 °C by a solar simulator (Wacom, model WXS-155S-L2). The external quantum efficiency (EQE) of the solar cells was characterized using a quantum efficiency measurement system (PV Measurement, QEW7).

Table 1
Deposition condition of i-a-$Si_{1-x}O_x$:H.

Parameters	Values	Unit
H_2/SiH_4	20	
CO_2/SiH_4	0–1	
Plasma frequency	27	MHz
Deposition temperature	160	°C
Deposition pressure	500	mTorr
Power density	250	mW/cm^2

3. Results and discussion

3.1. Effect of CO_2 flow rate variation on the optical and structural property of i-a-$Si_{1-x}O_x$:H films

In general, adding an oxygen (O) atom to the conventional a-Si:H material via CO_2 gas flowing during the plasma deposition increases the bandgap of the material [30,31]. A new material, a-$Si_{1-x}O_x$:H, was prepared. However, when adding O, the dangling bond (defect density) of this material is also increased with the increase of the CO_2 gas flow rate [30,31]. Therefore, balance is needed between the increasing of the material bandgap and the electrical properties.

Fig. 1 shows the Tauc plot of a-Si:H (film without CO_2 gas) and a-$Si_{1-x}O_x$:H films as a function of the CO_2 flow rate. In this experiment, the flow rate of CO_2 gas was varied from 0 to 4 sccm. It was found that E_{opt} of the a-$Si_{1-x}O_x$:H films was increased from 1.72 to 1.84 eV with increasing CO_2 gas flow rate. In general, E_{opt} of the a-$Si_{1-x}O_x$:H materials will be increased with the increase of the O and H concentrations. Evidence for this can be observed by FTIR spectrophotometry at wavenumbers of 900–1200 cm^{-1} and 1850–2250 cm^{-1} for O and H stretching modes, respectively [32,33].

Fig. 2 shows the FTIR measurement results of the a-$Si_{1-x}O_x$:H films deposited with and without CO_2 gas. It was found that E_{opt} of the a-$Si_{1-x}O_x$:H films in this experiment was mainly increased by the increase of O corresponding to the increasing of the CO_2 flow rate. However, increasing the CO_2 flow rate did not show a big impact on the H concentration of the films. E_{opt} of the a-$Si_{1-x}O_x$:H films was easily increased by increasing the CO_2 flow rate. However, the defect density of the films may be largely increased by increasing the CO_2 gas flow rate.

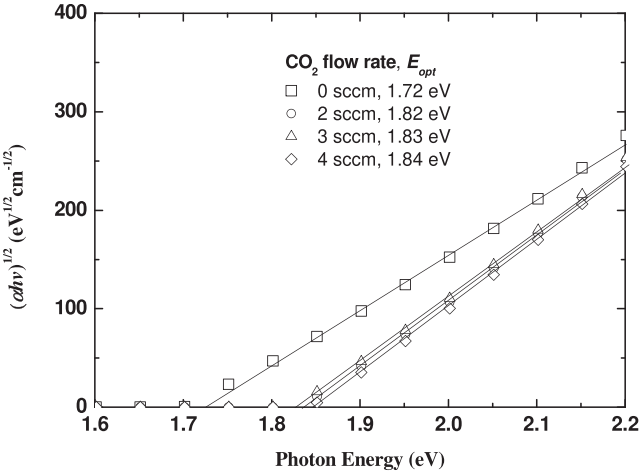

Fig. 1. E_{opt} of i-a-$Si_{1-x}O_x$:H films as a function of CO_2 flow rate.

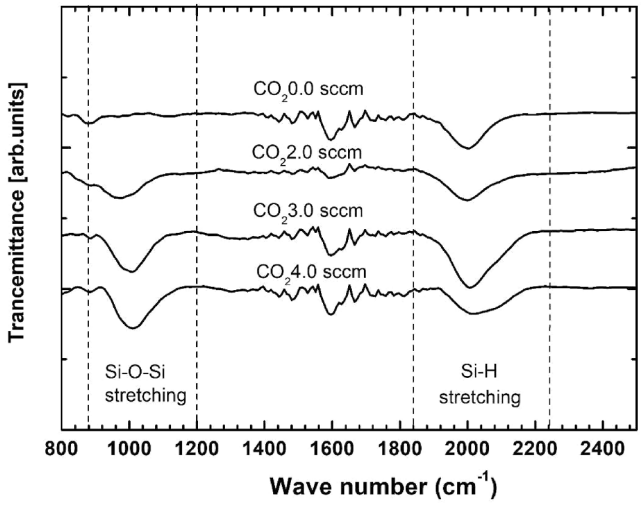

Fig. 2. FTIR absorption spectra of the a-$Si_{1-x}O_x$:H films as a function of CO_2 flow rate.

The films of this interface layer were deposited at the same deposition chamber as the n-type layer, and the defect density of the films is increased by not only the CO_2 flow rate but also the phosphine (PH_3) contamination inside the deposition chamber. Therefore, we kept the CO_2 gas flow rate in the low range to maintain the electrical properties of the a-$Si_{1-x}O_x$:H films. Fig. 3 shows the transmittance quality of the a-Si:H and a-$Si_{1-x}O_x$:H films as a function of the CO_2 gas flow rate. It was found that with increases of the CO_2 gas flow rate, the percentage of transmittance was increased at long wavelengths over 750 nm. From this result, it may be expected that by using the wide-bandgap a-$Si_{1-x}O_x$:H as the i/n interface layer of the a-$Si_{1-x}Ge_x$:H solar cell , the J_{sc} can be increased due to the higher reflectance from the back reflector material (ZnO:Al and Ag).

Fig. 4 shows the refractive index (n) of a-$Si_{1-x}O_x$:H films as a function of the CO_2 gas flow rate. When increasing the CO_2 gas flow rate, the refractive index of the film was decreased. These experimental results indicate that a-$Si_{1-x}O_x$:H is suitable for use as the i/n interface layer due to the high transparency and low reflectance. A part of the unabsorbed light or long-wavelength light can be reflected at the i/n interface back to the i-layer, thereby raising the possibility of additional absorption of the light in the absorbing layer [34].

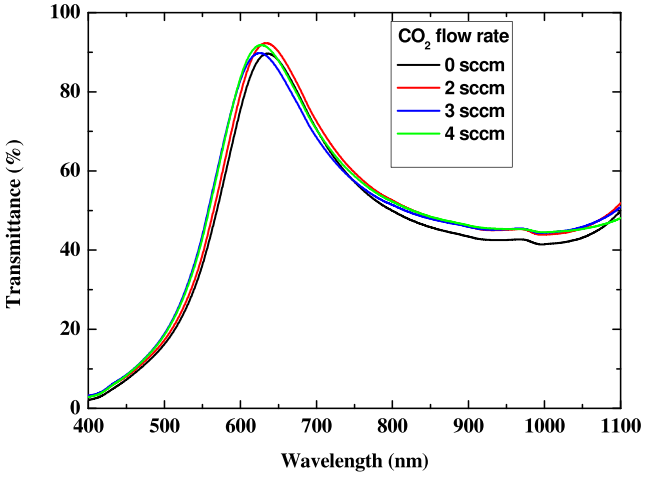

Fig. 3. Transmittance (%) of the a-$Si_{1-x}O_x$:H films as a function of CO_2 flow rate.

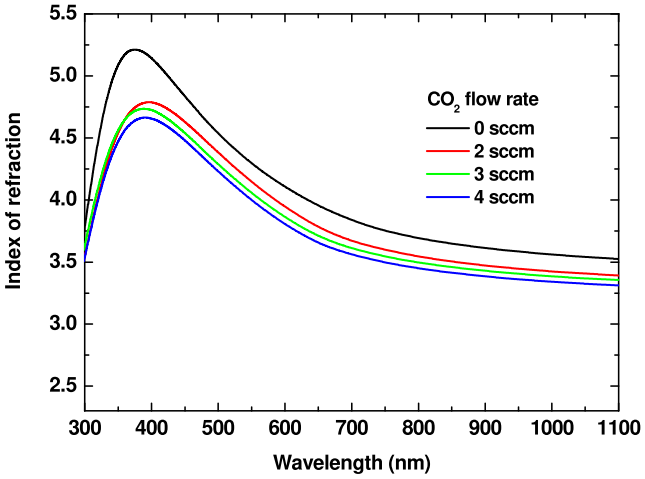

Fig. 4. Reflective index of i-a-$Si_{1-x}O_x$:H films as a function of CO_2 flow rate.

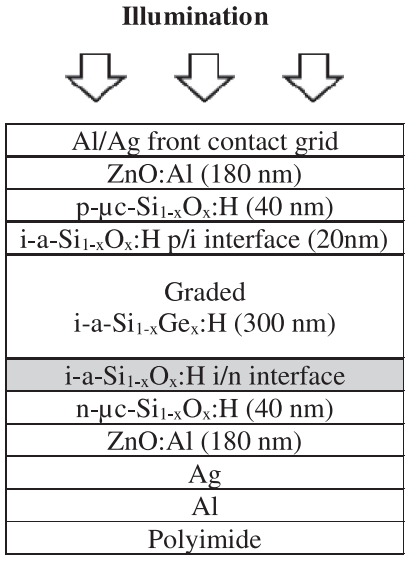

Fig. 5. Structure of a-$Si_{1-x}Ge_x$:H single-junction flexible solar cells.

3.2. Effects of CO_2 flow rate variation on i-a-$Si_{1-x}O_x$:H i/n interface layer of a-$Si_{1-x}Ge_x$:H single-junction flexible solar cells

To assess the role of the i/n interface layer in the performance of the cells, the variation of the CO_2 flow rate in the i/n interface layer was investigated. The structure of the solar cell consists of polyimide substrate/Al/Ag/ZnO:Al/n-μc-$Si_{1-x}O_x$:H/i-$Si_{1-x}O_x$:H i/n interface layer/VU-shape i-a-$Si_{1-x}Ge_x$:H bandgap profiling/i-$Si_{1-x}O_x$:H p/i interface layer/p-μc-$Si_{1-x}O_x$:H/ZnO:Al/Ag/Al front grid electrode. The structure and thickness of each layer are shown in Fig. 5. Fig. 6 shows the effect of the CO_2 flow rate variation on the i/n interface layer. In this case, we kept the thickness of the i/n interface layer at 20 nm. It was found that the open-circuit voltage (V_{oc}) of the solar cells increased from 0.795 to 0.805 V on average when increasing the CO_2 flow rate from 0 to 3.0 sccm. This result indicates that the increase of the bandgap of the i/n interface layer could improve the discontinuities that cause the lattice mismatch between the i and n-layers [8,13,21,34,35].

However, with a CO_2 flow rate of 3.5 sccm, V_{oc} tends to decrease to 0.790 V on average. From this result, we may conclude that with a high CO_2 flow rate, the bandgap discontinuities between the i and n-layers affect V_{oc} due to the bandgap of the i/n interface layer being too large. On the other hand, when increasing the CO_2 flow rate, the defect density

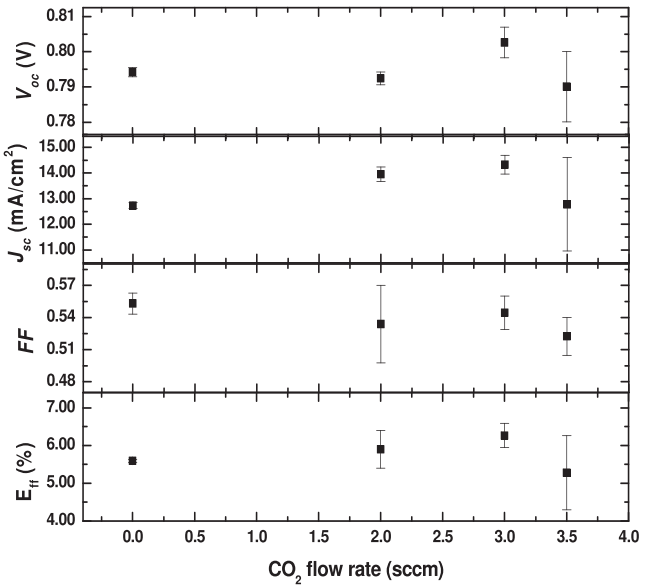

Fig. 6. Solar cells performance as a function of CO_2 flow rate.

of the i-$Si_{1-x}O_x$:H i/n interface-layer was increased passed the optimization point for use in the i/n interface region.

For the short circuit current density (J_{sc}), it was found that with increasing bandgap of the i/n interface layer, J_{sc} was increased on average from 13.0 to 14.5 mA/cm^2 for CO_2 flow rates of 0 to 3.0 sccm. The increase in J_{sc} is due to the higher transparency of the i/n interface, so the light can be reflected from the back reflector to the i-layer. This result is explained by the low parasitic absorption at the p/i interface, and the better collection of electron-hole pairs generated by the long wavelength was improved by improving the band discontinuity at the i/n interface [34]. However, with a CO_2 flow rate of 3.5 sccm, J_{sc} of the solar cell was decreased to 13.0 mA/cm^2. This result may be due to the decrease of the electron-hole pairs generated at the i/n interface with the increasing of the defect density of the i/n interface layer [34].

Fig. 7 shows the external quantum efficiency (EQE) of the sample selected from the highest J_{sc} of each CO_2 flow rate variation. It was found that the EQE was improved in the wavelength of 550 to 750 nm of the solar cell with CO_2 gas flow rates of 2.0 and 3.0 sccm at the i/n interface layers. In contrast, with a CO_2 flow rate of 3.5 sccm, the EQE at wavelengths of 550 to 750 nm was decreased, which may be due to the effect of the defect density of the i/n interface layer [34].

The fill factor (*FF*) is very sensitive to the defect density and the

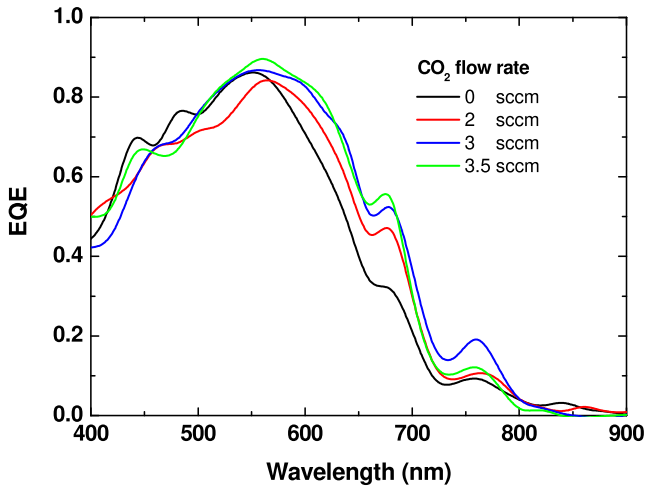

Fig. 7. External quantum efficiency of solar cells as a function of CO_2 flow rate.

bandgap discontinuities between the i and n-layers. With increasing CO_2 flow rate, *FF* tended to decrease from 0.57 to 0.54 on average. This result indicates that increasing the CO_2 flow rate for the a-$Si_{1-x}O_x$:H at the i/n interface layer causes an increase of the defect density in the i/n interface region. This result may show the disadvantage of using a-$Si_{1-x}O_x$:H as an i/n interface layer. When the overall solar cell performance was considered, it was found that using a-$Si_{1-x}O_x$:H as the i/n interface layer improved the conversion efficiency (E_{ff}) on average from 5.5 to 6.2% with increasing CO_2 flow rate from 0 to 3.0 sccm. The increase of E_{ff} was due to the higher J_{sc} and V_{oc} compared to those of the conventional a-Si:H i/n interface layer. However, with a CO_2 flow rate of 3.5 sccm, E_{ff} of the solar cell was decreased to 5.2% due the effect of V_{oc}, J_{sc}, and *FF*, which is attributed to the effect of the defect density and band discontinuity caused by a CO_2 flow rate that was too high.

To fine-tune E_{ff} of the solar cell, the effect of the i/n layer thickness was investigated. With a CO_2 flow rate over 2.0 sccm, *FF* of the solar cells sharply decreased. Thus, in this experiment, the CO_2 flow rate was kept constant at 2.0 sccm, while the thickness of the i/n interface layer thickness was varied from 10 to 40 nm. Fig. 8 shows the solar cell performance as a function of the i-$Si_{1-x}O_x$:H i/n interface layer thickness. It was found that the average V_{oc} slightly decreased from 0.80 to 0.78 V with the increase of the i-$Si_{1-x}O_x$:H i/n interface layer thickness due to the decrease of effective built-in potential (V_b) with respect to the thickness of the i/n interface layer. J_{sc} shows the same decreasing tendency of the average value from 13.5 to 13.0 mA/cm^2.

Fig. 9 shows the EQE of the sample selected from the highest J_{sc} of each layer thickness. The figure shows the decrease of the long wavelength absorption with the increase of the i/n interface layer thickness due to the loss of light that was absorbed at the i/n interface layer. *FF* of the solar cell as a function of the i/n interface thickness variation shows an almost constant value on average of around 0.55. This result indicates that with a small increase of the i/n interface layer thickness from 10 to 40 nm, the loss of V_b in this case did not affect *FF*. As a result, the conversion efficiency of the solar cell as a function of the i/n interface layer thickness shows a slight decrease from 6.0 to 5.5% on average. In conclusion, an a-$Si_{1-x}Ge_x$:H single-junction flexible solar cell with a maximum conversion efficiency (E_{ff}) of 6.6% (V_{oc} = 0.81 V, J_{sc} = 14.6 mA/cm^2 and *FF* = 0.57) was achieved.

4. Conclusions

The optical properties of i-a-$Si_{1-x}O_x$:H films deposited in an n-type

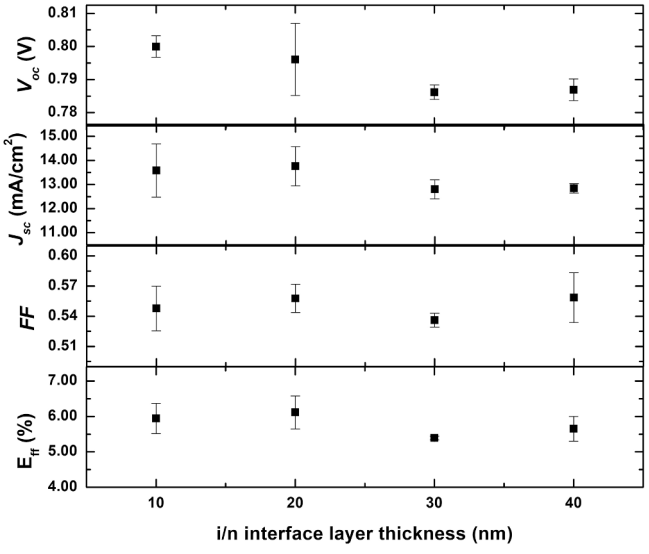

Fig. 8. Solar cells performance as a function of i/n interface layer thickness variation.

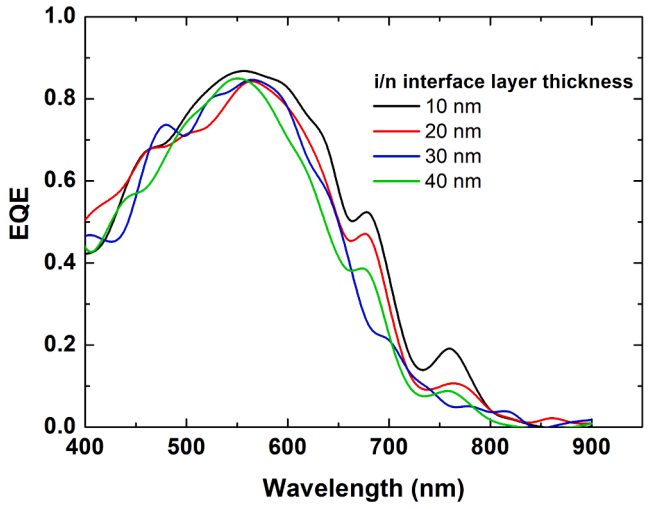

Fig. 9. External quantum efficiency of solar cells as a function of i/n interface layer thickness variation.

deposition chamber were investigated with low variation of the CO_2 flow rate. The optical bandgap, bonding structure, transparency properties, and reflective index were studied. The optical bandgap and transparency properties showed an opportunity for the application of the i/n interface layer in an a-$Si_{1-x}Ge_x$:H flexible solar cell. Solar cells were fabricated, and the results indicated that i-a-$Si_{1-x}O_x$:H is a candidate material for the i/n interface layer due to the increase of V_{oc} and J_{sc} of the solar cells.

The increase of V_{oc} could be attributed to the improvement of the discontinuities causing lattice mismatch between the i and n-layers, while the increase of J_{sc} was improved by the higher transparency of the i/n interface, so light could be reflected from the back reflector to the i-layer. The collection of electron-hole pairs generated by long wavelengths was also improved by improving the band discontinuity at the i/n interface. Finally, the variation of the i-a-$Si_{1-x}O_x$:H i/n interface layer thickness indicated that the solar cell performance tended to decrease with the increase of the i/n interface layer thickness due to the loss of effective built-in potential at the i/n interface layer.

Declaration of Competing Interest

The authors declare that they have no known competing financial interests or personal relationships that could have appeared to influence the work reported in this paper.

Acknowledgments

This work was supported by National Electronics and Computer Technology Center (NECTEC) THAILAND under Grant No. P1350323.

References

[1] Y. Ichikawa, T. Yoshida, T. Hama, H. Sakai, K. Harashima, Sol. Energy Mater. Sol. Cells 66 (2001) 107–115, https://doi.org/10.1143/JJAP.43.7976.
[2] M. Izu, T. Ellison, Sol. Energy Mater. Sol. Cells 78 (2003) 613–626, https://doi.org/10.1016/S0927-0248(02)00454-3.
[3] A. Banerjee, S. Guha, J. Appl. Phys. 69 (1991) 1030, https://doi.org/10.1063/1.347418.
[4] T. Söderström, F.-J. Haug, X. Niquille, C. Ballif, Prog. Photovolt. Res. Appl. 17 (2009) 165–176, https://doi.org/10.1002/pip.869.
[5] D.Y. Kim, E. Guijt, F.T. Si, R. Santbergen, J. Holovsky', O. Isabella, A.C.M.M. van Rene', M.Z. Swaaij, Sol. Energy Mater. Sol. Cells 141 (2015) 148–153, https://doi.org/10.1016/j.solmat.2015.05.033.
[6] J. Yang, A. Banerjee, S. Guha, Appl. Phys. Lett. 70 (1997) 2975–2977, https://doi.org/10.1063/1.118761.
[7] B. Yan, G. Yue, L. Sivec, J. Yang, S. Guha, C.-S. Jiang, Appl. Phys. Lett. 99 (2011), 113512, https://doi.org/10.1063/1.3638068.
[8] D.P. Pham, S. Kim, J. Park, J. Cho, H. Kim, A.H.T. Le, J. Yi, Optik Int. J. Light Elect. Opt. 136 (2017) 507e512, https://doi.org/10.1016/j.ijleo.2017.02.074.
[9] B.G. Budaguan, A.A. Sherchenkov, G.L. Gorbulin, V.D. Chernomordic, J. Phys. Condens. Matter 13 (2001) 6615–6624. http://iopscience.iop.org/0953-8984/13/31/303.
[10] S. Kim, J.W. Chung, H. Lee, J. Park, Y. Heo, H.M. Lee, Sol. Energy Mater. Sol. Cells 119 (2013) 26–35, https://doi.org/10.1016/j.solmat.2013.04.016.
[11] C. Ducros, H. Szambolics, F. Emieux, A. Pereira, Thin Solid Films 620 (2016) 10–16, https://doi.org/10.1016/j.tsf.2016.07.077.
[12] D.P. Pham, S. Kim, J. Park, A.H.T. Le, J. Cho, J. Yi, J. Alloys Compd. 724 (2017) 400–405, https://doi.org/10.1016/j.jallcom.2017.05.026.
[13] D. Lundszien, F. Finger, H. Wagner, Sol. Energy Mater. Sol. Cells 74 (2002) 365, https://doi.org/10.1016/S0927-0248(02)00096-X.
[14] R.J. Zambrano, F.A. Rubinelli, J.K. Rath, R.E.I. Schropp, J. Non-Cryst. Solids 1131 (2002) 299–302, https://doi.org/10.1016/S0022-3093(01)01080-8.
[15] R.J. Zambrano, F.A. Rubinelli, W.M. Arnoldbik, J.K. Rath, R.E.I. Schropp, Sol. Energy Mater. Sol. Cells 81 (2004) 73–86, https://doi.org/10.1016/j.solmat.2003.08.017.
[16] A. Gordijn, R.J. Zambrano, J.K. Rath, R.E.I. Schropp, IEEE Trans. Electron Devices 49 (2009) 3–14, https://doi.org/10.1149/1.3207570.
[17] J.-W. Chung, J.W. Park, Y.J. Lee, S.-W. Ahn, H.-M. Lee, O.O. Park, Jpn. J. Appl. Phys. 51 (2012) 10NB16. https://iopscience.iop.org/article/10.1143/JJAP.51.10NB16.
[18] S. Inthisang, T. Krajangsang, A. Hongsingthong, A. Limmanee, S. Kittisontirak, S. Jaroensathainchok, A. Moolakorn, A. Dousse, J. Sritharathikhun, K. Sriprapha, Jpn. J. Appl. Phys. 54 (2015) 08KB08. https://iopscience.iop.org/article/10.7567/JJAP.54.08KB08.
[19] E. Marins, M. Warzecha, S. Michard, J. Hotovy, W. Böttler, P. Alpuim, F. Finger, Thin Solid Films 571 (2014) 9–12, https://doi.org/10.1016/j.tsf.2014.09.026.
[20] A. Limmanee, P. Krudtad, S. Songtrai, C. Piromjit, J. Sritharathikhun, K. Sriprapha, Curr. Appl. Phys. 11 (2011) s206–s209, https://doi.org/10.1016/j.cap.2010.11.041.
[21] P. Pham, S. Kim, J. Parka, J. Cho, H.S. Kim, A.H.T. Le, J. Yi, Optik 136 (2017) 507–512, https://doi.org/10.1016/j.ijleo.2017.02.074.
[22] D.P. Pham, S. Kim, A.H.T. Le, J. Park, J. Yi, J. Alloys Compd. 762 (2018) 616–620, https://doi.org/10.1016/j.jallcom.2018.05.248.
[23] A. Idda, L. Ayat, N. Dahbi, O.J. Zaoui, Fundam. Appl. Sci. 12 (1S) (2020) 66–77. ISSN 1112-9867.
[24] K. Sriprapha, A. Hongsingthong, T. Krajangsang, S. Inthisang, S. Jaroensathainchok, A. Limmanee, W. Titiroongruang, J. Sritharathikhun, Thin Solid Films 546 (2013) 398–403, https://doi.org/10.1016/j.tsf.2013.05.137.
[25] J. Sritharathikhun, S. Inthisang, T. Krajangsang, A. Limmanee, K. Sriprapha, Thin Solid Films 546 (2013), https://doi.org/10.1016/j.tsf.2013.05.138.
[26] J. Tauc, Mater. Res. Bull. 3 (1968) 37–46, https://doi.org/10.1016/0025-5408(68)90023-8.
[27] L. Jarosinski, J. Pawlaka, S.K.J. Al-Anic, Opt. Mater. 88 (2019) 667–673, https://doi.org/10.1016/j.optmat.2018.12.041.
[28] E. Marins, M. Warzecha, S. Michard, J. Hotovy, W. Böttler, P. Alpuim, F. Finger, Thin Solid Films 571 (2014) 9–12, https://doi.org/10.1016/j.tsf.2014.09.026.
[29] A.V. Shah, H. Schade, M. Vanecek, J. Meier, E. Vallat-Sauvain, N. Wyrsch, U. Kroll, C. Droz, J. Bailat, Prog. Photovolt.: Res. Appl. 12 (2004) 113–142, https://doi.org/10.1002/pip.533.
[30] A. Janotta, R. Janssen, M. Schmidt, T. Graf, M. Stutzmann, L. Görgens, A. Bergmaier, G. Dollinger, C. Hammerl, S. Schreiber, B. Stritzker, Phys. Rev. B 69 (2004), 115206, https://doi.org/10.1103/PhysRevB.69.115206.
[31] S. Wang, V. Smirnov, T. Chen, B. Holländer, X. Zhang, S. Xiong, Y. Zhao, F. Finger, Jpn. J. Appl. Phys. 54 (2014), 011401, https://doi.org/10.7567/JJAP.54.011401.
[32] S.M. Iftiquar, High Temp. Mater. Process. 6 (2002) 35–53. arXiv:cond-mat/0305636.
[33] K. Haga, H. Watanabe, J. Non-Cryst. Solids 195 (1996) 72–75, https://doi.org/10.1016/0022-3093(95)00544-7.
[34] C. Shin, S.M. Iftiquar, J. Park, Y. Kim, S. Kim, J. Jung, J. Yi, Mater. Sci. Semicond. Process. 66 (2017) 223–231, https://doi.org/10.1016/j.mssp.2017.05.002.
[35] J. Park, V.A. Dao, S. Kim, D.P. Pham, S. Kim, A.H.T. Le, J. Kang, J. Yi, Sci. Rep. 8 (2018) 15386. https://www.nature.com/articles/s41598-018-33734-y.